2010 IEEE International Conference on Robotics and Automation
Anchorage Convention District
May 3-8, 2010, Anchorage, Alaska, USA

# Real-time 3D Model-based Tracking Using Edge and Keypoint Features for Robotic Manipulation

Changhyun Choi and Henrik I. Christensen
Robotics & Intelligent Machines, College of Computing
Georgia Institute of Technology
Atlanta, GA 30332, USA
{cchoi,hic}@cc.gatech.edu

*Abstract*— **We propose a combined approach for 3D real-time object recognition and tracking, which is directly applicable to robotic manipulation. We use keypoints features for the initial pose estimation. This pose estimate serves as an initial estimate for edge-based tracking. The combination of these two complementary methods provides an efficient and robust tracking solution. The main contributions of this paper includes: 1) While most of the RAPiD style tracking methods have used simplified CAD models or at least manually well designed models, our system can handle any form of polygon mesh model. To achieve the generality of object shapes, salient edges are automatically identified during an offline stage. Dull edges usually invisible in images are maintained as well for the cases when they constitute the object boundaries. 2) Our system provides a fully automatic recognition and tracking solution, unlike most of the previous edge-based tracking that require a manual pose initialization scheme. Since the edge-based tracking sometimes drift because of edge ambiguity, the proposed system monitors the tracking results and occasionally re-initialize when the tracking results are inconsistent. Experimental results demonstrate our system's efficiency as well as robustness.**

## I. Introduction

As robots moves from industrial to daily environments, the most important problem robots face is to recognize objects and estimate 6-DOF pose parameters in less constrained environments. For the last decade, computer vision, robotics, and augmented reality have all addressed this as a model-based tracking issue. Most of the work has been based on 3D CAD models or keypoint metric models. The former models correspond to edges in an image, which can be efficiently computed, while the latter models match with keypoints in an image which are suitable for robust wide baseline matching. A strategy for using keypoint for pose initialization and differential methods for pose tracking is presented.

## II. Related Work

For the 6-DOF pose tracking, robotics and augmented reality areas have employed a number of different approaches. One of the easiest way is through use of fiducial markers. Artificial markers are attached to the object or environment as camera targets. Although the method provides an easy and robust solution for real-time pose estimation, attaching markers has been regarded as a major limitation. Hence, researchers have focused on tracking using natural features. For several decades methods, which employ natural features, have been proposed: *edge-based*, *optical flow-based*, *template-based*, and *keypoint-based*. Each method has its own pros and cons, but surveying every methods in this paper is out of scope. For an in-depth study of the different methods, we refer the interested reader to the survey [1].

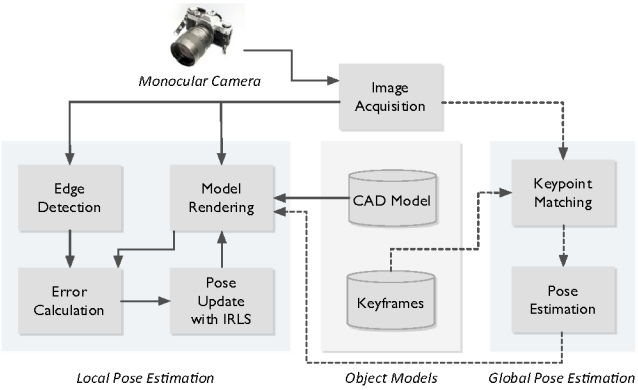


Fig. 1: Overall system flow. We use a monocular camera. The initial pose of the object is estimated by using the SURF keypoint matching in the Global Pose Estimation (GPE). Using the initial pose, the Local Pose Estimation (LPE) consecutively estimates poses of the object utilizing RAPiD style tracking. keyframes and CAD model are employed as models by the GPE and LPE, respectively. The model are generated offline.

Among the various methods, we focus on two methods: *edge-based* and *keypoint-based*. The edge features are easy to compute and computationally cheap. Since the edge is usually computed by image gradients, it is moderately invariant to illumination and viewpoint. The keypoint features are also capable of being invariant to illumination, orientation, scale, and partially viewpoint. But the keypoints requires relatively computationally expensive descriptors which maintain local texture or orientation information around stable points to be distinctive.

In *edge-based* methods, a 3D CAD model is usually employed to estimate the full pose using a monocular camera. Harris [2] established RAPiD (Real-time Attitude and Position Determination) which was one of the first marker-less 3D model-based real-time tracking system. It tracks an object by comparing projected CAD model edges to edges detected in a gray-scale image. To project the model close

Fig. 2: Example keyframes of the teabox object. The keyframes are saved during offline analysis and later utilized in the GPE.

to the real object, the system use the previous pose estimate as a priori. Since it use an 1-D search along the normal direction of sample points for the closest edge locations, it rapidly calculate errors which must be minimized to solve for the 6-DOF motion parameters. The motion parameters are subsequently estimated between frames. Drummond and Cipolla [3] solved a similar problem, but enhanced robustness by using the iterative re-weighted least squares with a M-estimator. To perform hidden line removal, they used a BSP (Binary Space Partition) tree. Marchand and Chaumette [4] proposed an augmented reality framework, which relies on points and lines, and that has been applied to the visual servoing [5]. Comport *et al.* [6] compared and evaluated the two different systems, but they concluded both are fundamentally equivalent.

In *keypoint-based* methods, a sparse 3D metric model is used. Like CAD models, the keypoint models are built offline. With a set of images in each has a view of an object from a slightly different viewpoint, the non-linear optimization algorithm, such as Levenberg-Marquardt, return a refined 3D model of keypoints. Since this model maintains 3D coordinates of each keypoint, the pose estimation is easily performed by using the correspondence between the 3D points of the model and the 2D keypoints in an input image. Using this model, Gordon and Lowe [7] proposed an augmented reality system that calculates pose with scale invariant features [8]. Collet *et al.* [9] applied a similar method to robot manipulation where they combined RANSAC [10] with a clustering algorithm to locate multiple instances. Vacchetti *et al.* [11] used standard corner features to match the current image and the reference frames, so called keyframes. Unlike the efforts using non-linear optimization, they obtained 3D coordinates of 2D corner points by back-projecting them onto the object CAD model.

Since the edge and the keypoint methods are complementary to each other, several have reported combined approaches [12], [13]. Vacchetti *et al.* [14] incorporated the edge-based method with their corner point-based method to make the system more robust and jitter free. As part of the edge-based tracking, they used multiple hypotheses to handle erroneous edge correspondence, but it is equivalent to the nearest hypothesis of RAPiD-like approaches. Rosten and Drummond [15] similarly combined corner points with lines, but they only used corner points to estimate motion parameters between frames.

We also adopt a combined approach in which *keypoint-based* matching and *edge-based* tracking are employed. As depicted in Fig. 1, our system is composed of a Global Pose Estimation (GPE) and a Local Pose Estimation (LPE). Unlike [14] and [15] which use keypoints to estimate motion between frames, we only use the keypoints for estimating the initial pose in GPE. After estimating the initial pose an edge-based tracking scheme is utilized in the LPE.

In the remainder of the paper, we first explain the GPE in Section III. Section IV describes the LPE including the salient edge selection from polygon mesh models and the edge-based tracking formulation. Quantitative and qualitative results using the system are presented in Section V.

## III. Global Pose Estimation using keypoints

In this section, we present the Global Pose Estimation (GPE) in which we use SURF keypoints [16] to match the current image with keyframes. The model keyframe is a set of images that contains a target object. The keyframes are saved offline. To estimate pose, the 3D coordinate of each keypoint is computed by back-projecting to the CAD model.

### A. Keyframe Model Acquisition

To estimate an initial pose, our system requires keyframes, which are reference images. Since the keyframes will be compared with the input image, the keyframes should contain appearance of the object similar to the one in the input image. But it is practically impossible to maintain every image to cover all possible appearances of the object due to variability across illumination, scale, orientation and viewpoint. In a real application, a smaller number of keyframes is preferred. Ideally there would only be one keyframe per aspect for the object. For the maximum coverage of a keyframe, a keypoint descriptor that describes local appearance around corner-like points is used. If the local descriptor is discriminative then matching keypoints between two images can be performed despite variations in orientation, scale, and illumination. However, the local appearance is only semi-invariant to viewpoint change. For robust pose initialization we are required to maintain multiple keyframes to cover multiple view aspects.

Capturing keyframes is performed offline. Since keyframes will be used for pose estimation in which there is a need for generation of 2D-3D correspondences, we need to know the 3D coordinates of each keypoint. To calculate 3D coordinates, we use 3D CAD models with the current pose estimate. In this phase, the current pose is estimated by the LPE as will be explained in Section IV. With a CAD model and the current pose, we can compute the 3D coordinates of each keypoint by back-projecting the 2D keypoint to

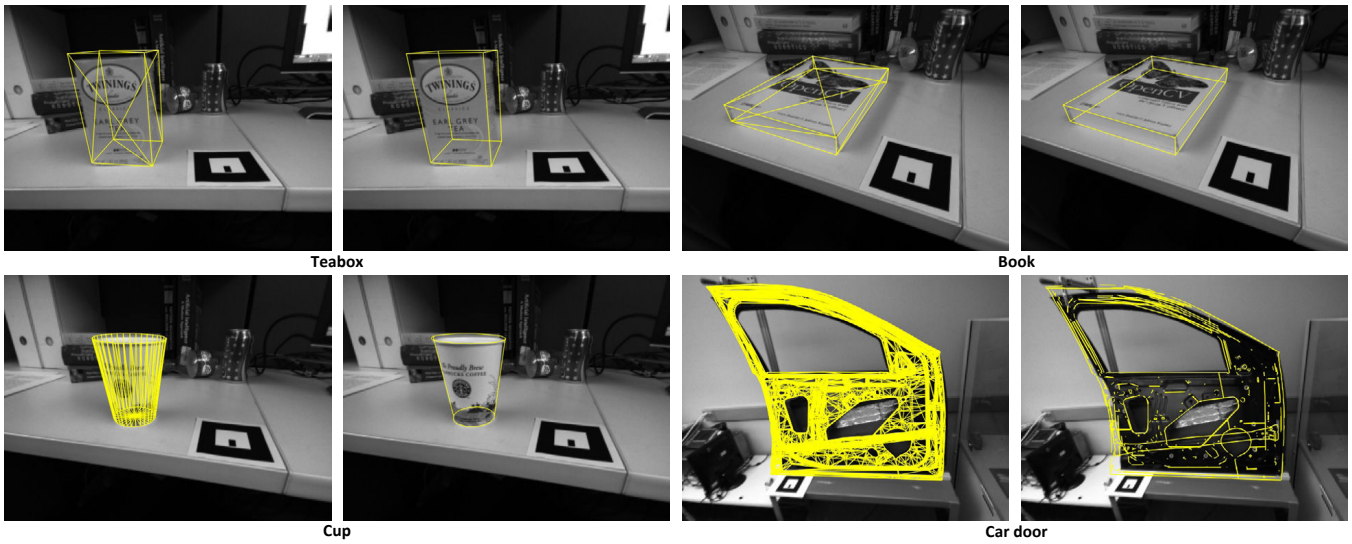


Fig. 3: Original and simplified CAD models. By using the salient edges selection, we can get a set of good model edges to track.

the corresponding facet of the CAD model. For fast facet identification, we use 'Facet-ID' trick which encodes i-th facet of the target object's model in an unique color in order to identify the membership of each 2D keypoints by looking up the image buffer that OpenGL renders [11]. The 3D coordinates of the keypoints are then saved into a file for later use in keypoint matching.

### B. Matching keypoints

After obtaining keyframes offline, keypoint matching is performed between an input frame and keyframes. A simple strategy for the matching might use naïve exhaustive search. However, such a search has $O(n^2)$ complexity. Using an approximate method the complexity can be reduced. As an approximated search, we use the Best-Bin-First (BBF) algorithm [17] which can be performed in $O(n \log n)$. While [18] and [8] used a fixed number of nearest-neighbors, we set the number of nearest-neighbors as the number of keyframe + 1. We use the ratio test described by [8], and the ratio threshold we used was 0.7. Once the putative correspondences has been determined, they are further refined using RANSAC [10]. In each RANSAC iteration, we estimate a homography matrix and eliminate outliers from the homography matrix. Since general objects have multiple faces or even curved surface, using the homography matrix might not be an optimal solution. It is here assumed that correspondences can be approximated by a plane to plane transformation. In addition, the size of objects is relatively small in images, so this approximation does not limit the number of correspondences. Another solution would be estimating a camera projection matrix directly as part of the RANSAC as we know 3D coordinates of each 2D keypoint, an option that may be considered in future work. After removing outliers, we then calculate the 6-DOF pose parameters by using standard least square estimation. This pose estimate is provided to the LPE as an initial value.

## IV. Local Pose Estimation using Edges

In this section, we explain the Local Pose Estimation (LPE) in which edges are utilized for object tracking.

### A. Automatic Salient Model Edges Selection

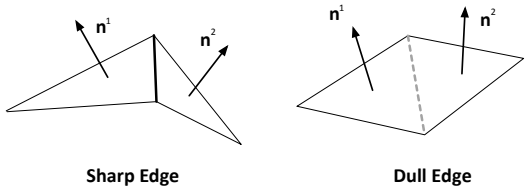


Fig. 5: Determining salient edges. We use the face normal vectors available in the model.

Since most of objects which exist in our daily environment are manufactured, their CAD models might be available, and such models provide helpful information for robotic manipulation. Although there are various formats in CAD models, most of them can be represented in a polygon mesh. A polygon mesh is usually composed of *vertices*, *edges*, *faces*, *polygons* and *surfaces*. In the LPE, we use edge features in images coming from a monocular camera to estimate the pose difference between two consecutive frames. So we should determine which *edges* in the model of a targeted object would be visible in images. Here we make an assumption that sharp edges are more likely to be salient. To identify sharp edges, we use the face normal vectors from the model. As illustrated in Fig. 5, if the face normal vectors of two adjacent faces are close to perpendicular, the edge shared by the two faces is regarded a sharp edge. If two face normal vectors are close to parallel, the edge is regarded a dull edge. For the decision, we use a simple thresholding scheme with the value of the inner product of two normal vectors. More formally, we can define an indicator function with respect to

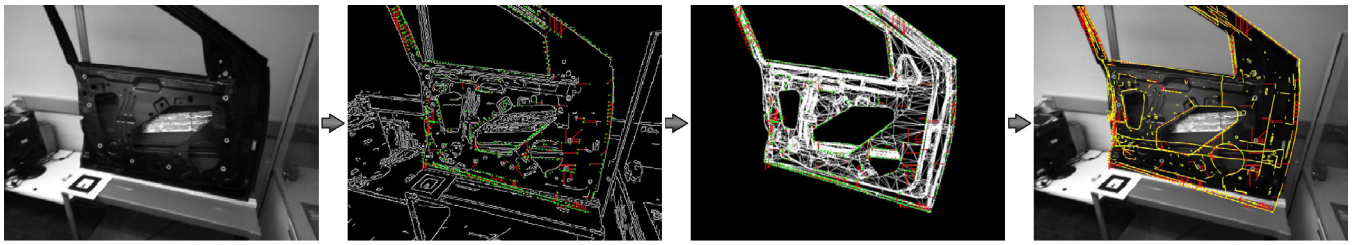

Fig. 4: The flow of the LPE. From the input image, an edge image is obtained using the Canny edge detector, and the CAD model is rendered with the prior pose. After calculate the error between the projected model and edge image, Iterative Re-weighted Least Square estimates the posterior pose. The estimated pose is shown in the last image.

the edges in the model by:

$$I(edge_i) = \begin{cases} 1 & \text{if } |\mathbf{n_i^1} \cdot \mathbf{n_i^2}| \leq \tau_s \\ 0 & \text{otherwise} \end{cases}$$

where $\mathbf{n_i^1}$ and $\mathbf{n_i^2}$ are the face normal unit vectors of the two adjacent faces which share the i-th edge, $edge_i$. We found the threshold $\tau_s = 0.3$ is a reasonable value. This salient edge selection is performed fully automatically offline. In general, the salient edges are only considered in edge-based tracking, but when the dull edges constitute the object's boundary they are also considered. Testing boundary of the dull edges are performed at run-time using back-face culling.

### B. Mathematical and Camera Projection Model

Since our approach is based on the formulation from Drummond and Cipolla [3], we adopt the Lie Algebra formulation. In the LPE, our goal is to estimate the posterior pose $E_{t+1}$ from the prior pose $E_t$ given the inter-frame motion $M$:

$$E_{t+1} = E_t M$$

where $E_{t+1}$, $E_t$, and $M$ are 6-dimensional Lie Group of rigid body motion in $SE(3)$. At time $t+1$, we know the prior pose $E_t$ from the GPE or the previous LPE. Hence we are interested in determining the motion $M$ to estimate the posterior pose. $M$ can be represented in the exponential map of generators $G_i$ as follows:

$$M = \exp(\boldsymbol{\mu}) = e^{\sum_{i=1}^{6} \mu_i G_i} \tag{1}$$

where $\boldsymbol{\mu} \in \mathbb{R}^6$ is the motion velocities corresponding to the 6-DOF instantaneous displacement and the $G_i$ are the group generator matrices:

$$G_1 = \begin{pmatrix} 0&0&0&1 \\ 0&0&0&0 \\ 0&0&0&0 \\ 0&0&0&0 \end{pmatrix}, G_2 = \begin{pmatrix} 0&0&0&0 \\ 0&0&0&1 \\ 0&0&0&0 \\ 0&0&0&0 \end{pmatrix}, G_3 = \begin{pmatrix} 0&0&0&0 \\ 0&0&0&0 \\ 0&0&0&1 \\ 0&0&0&0 \end{pmatrix},$$

$$G_4 = \begin{pmatrix} 0&0&0&0 \\ 0&0&-1&0 \\ 0&1&0&0 \\ 0&0&0&0 \end{pmatrix}, G_5 = \begin{pmatrix} 0&0&1&0 \\ 0&0&0&0 \\ -1&0&0&0 \\ 0&0&0&0 \end{pmatrix}, G_6 = \begin{pmatrix} 0&-1&0&0 \\ 1&0&0&0 \\ 0&0&0&0 \\ 0&0&0&0 \end{pmatrix}.$$

As a camera model, we use the standard pin-hole model given by:

$$\mathbf{p} = \text{Proj}(\mathbf{P^M}; E, K) = K \begin{pmatrix} \frac{x^C}{z^C} \\ \frac{y^C}{z^C} \\ 1 \end{pmatrix} \tag{2}$$

where $\mathbf{p} = (u\ v)^T$ is 2D image coordinates corresponding to the 3D model coordinates $\mathbf{P^M} = (x^M\ y^M\ z^M\ 1)^T$ and the matrix $K$ represent the camera's intrinsic parameters:

$$K = \begin{pmatrix} f_u & 0 & u_0 \\ 0 & f_v & v_0 \end{pmatrix}$$

where $f_u$ and $f_v$ are the focal length in pixel dimensions, and $u_0$ and $v_0$ represent the position of the principal point. The 3D coordinates in camera coordinates $\mathbf{P^C} = (x^C\ y^C\ z^C\ 1)^T$ can be calculated by:

$$\mathbf{P^C} = E\mathbf{P^M}$$

where $E$ is the extrinsic matrix or camera's pose. For simplicity, we ignore the radial distortion as image rectification is performed during the image acquisition phase.

### C. Model Rendering and Error Calculation

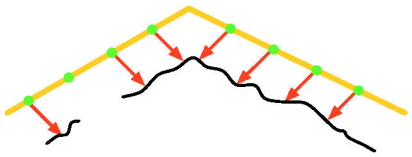

Fig. 7: Error calculation between projected model (yellow lines) and extracted edges (black tortuous lines) from the input image. Sample points (green points) are generated along the model per fixed distance, the error of each sampled point is calculated by the 1-D search along the direction orthogonal to the model edge.

To estimate the motion $M$, we need to measure errors between the prior pose and the current pose. As a first step to calculate errors, we project the CAD model to the image plane using the prior pose $E_t$. Instead of considering the edge itself, we sample points along the projected edges. Since some of sampled points are occluded by the object itself, a visibility test is performed. While [3] used a BSP tree for hidden line removal, OpenGL occlusion query is an easy and efficient alternative. Each visible point is then matched to the edges in the input image. The edge image is obtained by using a Canny Edge Detector [19]. We find the nearest edge by using a 1-D search along the direction perpendicular to the projected edge. The error vector $\mathbf{e}$ is obtained by stacking all of the errors of each sample point as follows:

$$\mathbf{e} = (e_1\ e_2\ \ldots\ e_N)^T$$

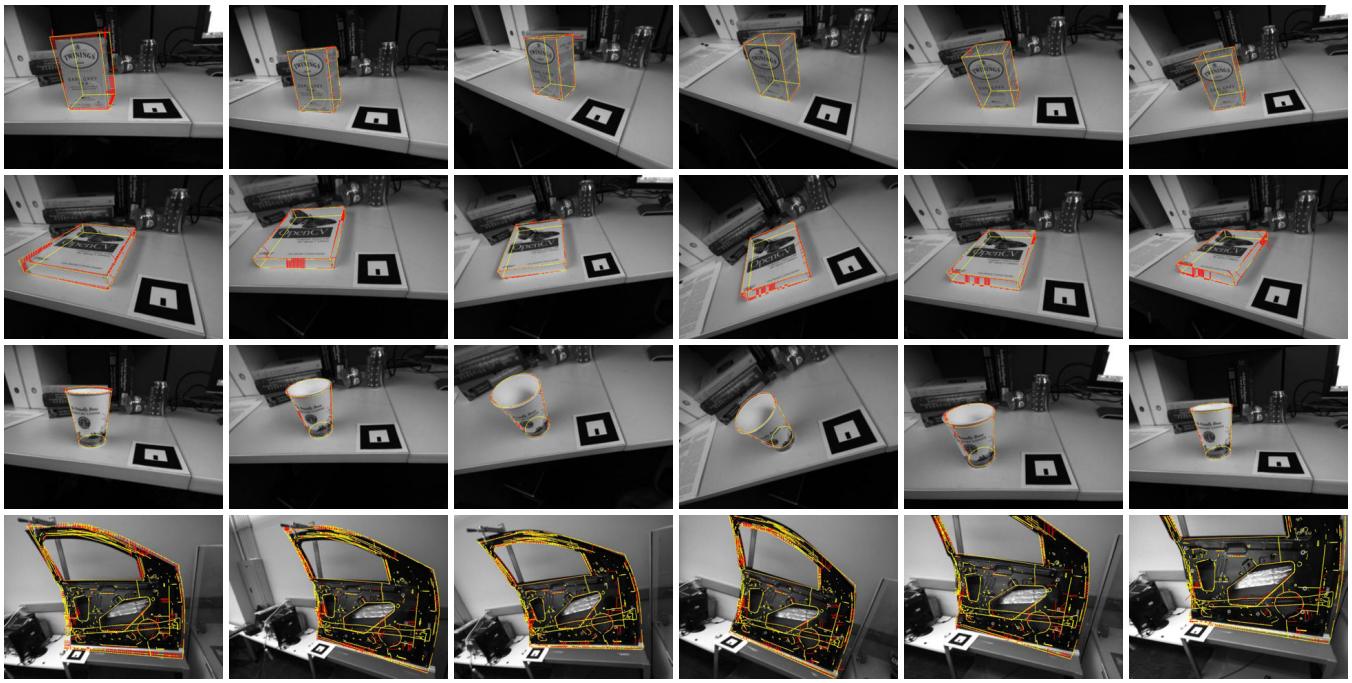

Fig. 6: Tracking results of the four targeted objects. From top to bottom, teabox, book, cup and car door. From left to right, t $<$ 10, t = 100, t = 200, t = 300, t = 400 and t = 500 where t is the frame number. The very left images are results of the GPE.

where $e_i$ is the Euclidean distance from i-th sample point to the nearest edge and $N$ is the number of valid sample points (i.e. sample points correspond to the nearest edge). Fig. 7 illustrates the error calculation, and $e_i$ is the length of the i-th red arrow.

### D. Update Pose with IRLS

After calculating the error vector $\mathbf{e}$, the problem is reduced to:

$$\begin{aligned}\hat{\boldsymbol{\mu}} &= \arg\min_{\boldsymbol{\mu}} \sum_{i=1}^{N} \|\mathbf{e_i}\|^2 \\ &= \arg\min_{\boldsymbol{\mu}} \sum_{i=1}^{N} \|\mathbf{p_i} - \mathrm{Proj}(\mathbf{P_i^M}; E_t \exp(\boldsymbol{\mu}), K)\|^2\end{aligned}$$

where $\mathbf{p_i}$ is the 2D image coordinates of the nearest edge which is corresponding to the projected 2D point of the i-th 3D model coordinates $\mathbf{P_i^M} = (x_i^M \ y_i^M \ z_i^M \ 1)^T$ and $N$ is the number of valid sample points.

To calculate $\boldsymbol{\mu}$ which minimizes the error $\mathbf{e}$, a Jacobian matrix $J \in \mathbb{R}^{N\times 6}$ can be obtained by computing partial derivatives at the current pose:

$$\begin{aligned}J_{ij} &= \frac{\partial e_i}{\partial \mu_j} \\ &= \mathbf{n_i}^T \frac{\partial}{\partial \mu_j} \begin{pmatrix} u_i \\ v_i \end{pmatrix} \\ &= \mathbf{n_i}^T \frac{\partial}{\partial \mu_j} \Big( \mathrm{Proj}(\mathbf{P_i^M}; E_t \exp(\boldsymbol{\mu}), K) \Big)\end{aligned}$$

where $\mathbf{n_i}$ is the unit normal vector of the i-th sample point.

We can split $\mathrm{Proj}()$ in Eq. 2 into two parts as follows:

$$\begin{pmatrix} u_i \\ v_i \end{pmatrix} = \begin{pmatrix} f_u & 0 & u_0 \\ 0 & f_v & v_0 \end{pmatrix} \begin{pmatrix} \tilde{u_i} \\ \tilde{v_i} \\ 1 \end{pmatrix}$$

$$\begin{pmatrix} \tilde{u_i} \\ \tilde{v_i} \end{pmatrix} = \begin{pmatrix} \frac{x_i^C}{z_i^C} \\ \frac{y_i^C}{z_i^C} \end{pmatrix}$$

Their corresponding Jacobian matrices can be obtained:

$$J_K = \begin{pmatrix} \frac{\partial u_i}{\partial \tilde{u_i}} & \frac{\partial u_i}{\partial \tilde{v_i}} \\ \frac{\partial v_i}{\partial \tilde{u_i}} & \frac{\partial v_i}{\partial \tilde{v_i}} \end{pmatrix} = \begin{pmatrix} f_u & 0 \\ 0 & f_v \end{pmatrix}$$

$$J_P = \begin{pmatrix} \frac{\partial \tilde{u_i}}{\partial x_i^C} & \frac{\partial \tilde{u_i}}{\partial y_i^C} & \frac{\partial \tilde{u_i}}{\partial z_i^C} \\ \frac{\partial \tilde{v_i}}{\partial x_i^C} & \frac{\partial \tilde{v_i}}{\partial y_i^C} & \frac{\partial \tilde{v_i}}{\partial z_i^C} \end{pmatrix} = \begin{pmatrix} \frac{1}{z_i^C} & 0 & -\frac{x_i^C}{(z_i^C)^2} \\ 0 & \frac{1}{z_i^C} & -\frac{y_i^C}{(z_i^C)^2} \end{pmatrix}$$

Since $\frac{\partial}{\partial \mu_j}(\exp(\boldsymbol{\mu})) = G_j$ at $\boldsymbol{\mu} = \mathbf{0}$ by Eq. 1, we can get:

$$\begin{aligned}\frac{\partial \mathbf{P_i^C}}{\partial \mu_j} &= \frac{\partial}{\partial \mu_j}(E_t \exp(\boldsymbol{\mu}) \mathbf{P_i^M}) \\ &= E_t G_j \mathbf{P_i^M}\end{aligned}$$

Therefore the $i^{th}$ row and $j^{th}$ column element of the Jacobian matrix $J$ is:

$$J_{ij} = \frac{\partial e_i}{\partial \mu_j} = \mathbf{n_i}^T J_K \begin{pmatrix} J_P & 0 \\ 0 & 0 \end{pmatrix} E_t G_j \mathbf{P_i^M}$$

We can solve the following equation to calculate the motion velocities:

$$J\boldsymbol{\mu} = \mathbf{e}$$

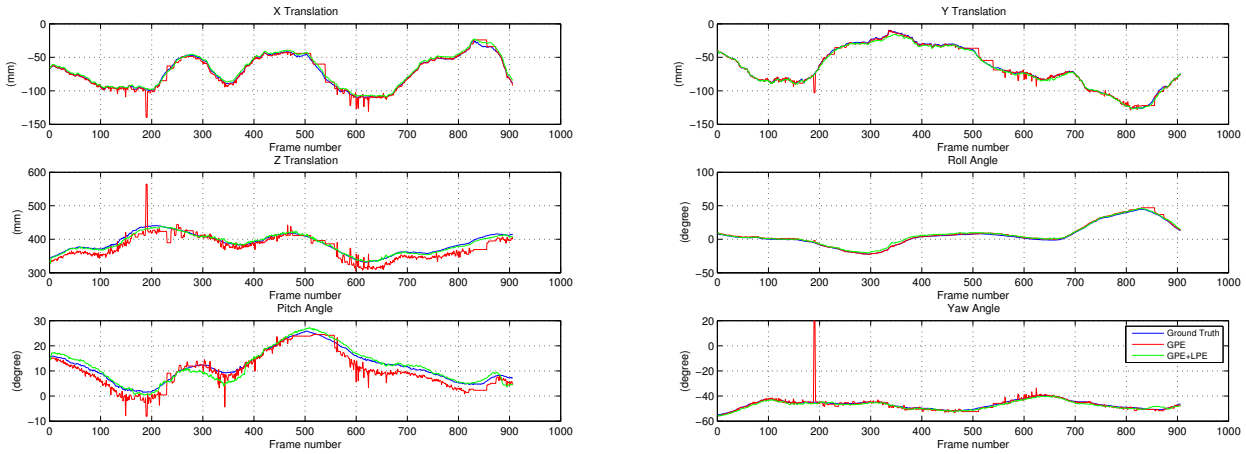


Fig. 8: 6-DOF pose plots of the book object in the general tracking test. While our approach (GPE+LPE) has convergence to ground truth, the GPE only mode suffers from jitter and occasionally fails to estimate pose.

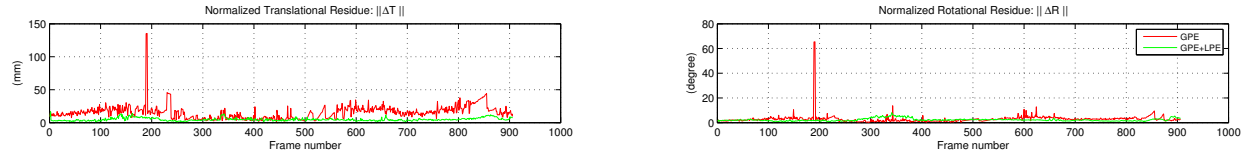


Fig. 9: Normalized residue plots of the book object in the general tracking test. The jitter and tracking failures result in a high residual.

Rather than using the usual pseudo-inverse of $J$, we solve the above equation with Iterative Re-weight Least Square (IRLS) and M-estimator:

$$\hat{\boldsymbol{\mu}} = (J^T W J)^{-1} J^T W \mathbf{e}$$

where $W$ is a diagonal matrix determined by a M-estimator. The i-th diagonal element in $W$ is $w_i = \frac{1}{c+e_i}$ where $c$ is a constant.

## V. Experimental Results

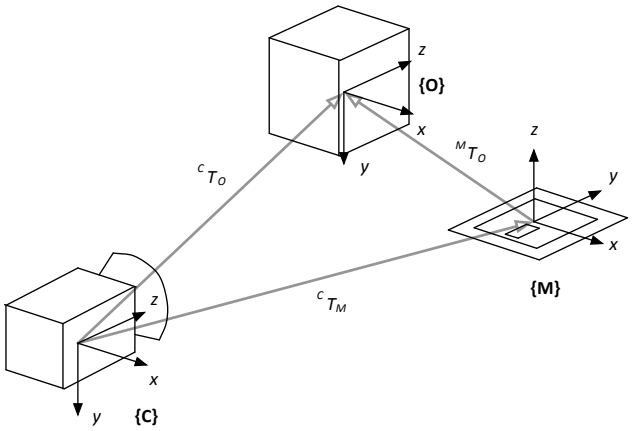


Fig. 10: Experimental setting and transformations between camera {C}, object {O} and marker {M} frames. We used AR markers to compute the ground truth pose.

In this section, we validate our visual recognition and tracking algorithm with several experiments. To show the generality of our system, we performed experiments with 4 objects: teabox, book, cup and car door. Note that these objects have different complexity and characteristics. The first three objects are especially interesting in for service robotics while the last object is of interest for assembly robots.

Our system is composed of a standard desktop computer and a Point Grey Research's Flea 1394 camera ($640 \times 480$ resolution). The CAD models of teabox, book and cup were generated by using Blender$^{TM}$ which is an open source 3D modeling tool. The car door model was provided by an automobile company. We converted all of the models to the OBJ format[1] to be used in our C++ implementation.

For the GPE, we prepared keyframe images. As a smaller number of keyframes is desirable, we captured only five keyframes per object. Each keyframe has different appearances of object as shown in Fig. 2.

### A. General Tracking Test

The tracking results for the four objects are shown in Fig. 6. The images in left-most column show estimated pose from the GPE and the last of them depicts the pose estimated by the LPE. Note that although the pose estimated by the GPE is not perfect, the subsequent LPE corrects the error and the pose estimates converge to the real pose. For quantitative evaluation, we employed AR markers to gather ground truth pose data. As shown in Fig. 10, we manually measured the transformation $^{M}T_{O}$ which is the description of the object frame $\{\mathbf{O}\}$ relative to the marker frame $\{\mathbf{M}\}$. So the ground

[1]OBJ format is developed by Wavefront Technologies and has been widely accepted for 3D graphics. That format can be easily handled by using the GLUT library.

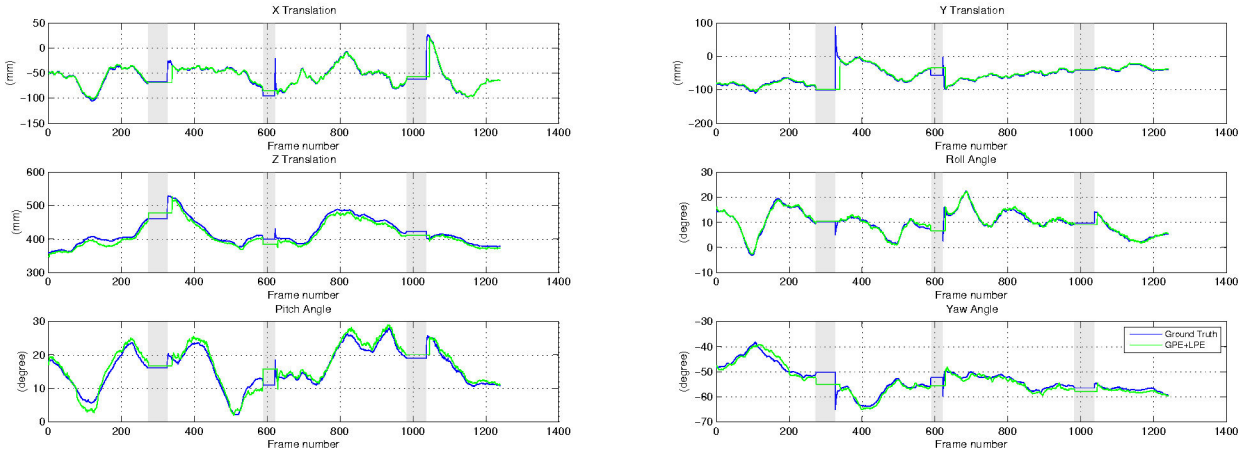


Fig. 11: 6-DOF pose plots of the book object in the re-initialization test. The shaded spans mean that the object and the marker are invisible because of fast camera movement or occlusion. Our approach (GPE+LPE) takes more frame to re-initialize than the AR marker, but it maintains track of the object.

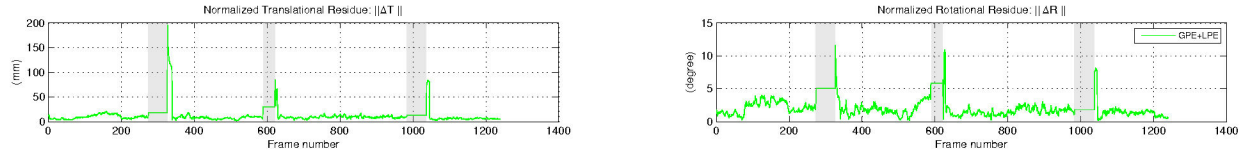


Fig. 12: Normalized residual plots of the book object in the re-initialization test. The three peaks are due to a time difference between the AR marker and our approach.

truth pose ${}^{C}T_{O}^{*}$ can be obtained as follows:

$$ {}^{C}T_{O}^{*} = {}^{C}T_{M}\ {}^{M}T_{O} $$

where ${}^{C}T_{M}$ is the pose estimated by AR markers. The estimated pose by our system ${}^{C}T_{O}$ is compared with the ground truth ${}^{C}T_{O}^{*}$ as shown in Fig. 8 and Fig. 11. The plot shows the estimated poses of the book object from the GPE only mode and the GPE+LPE mode. Since the GPE relies on the keypoint matching, the quality of the keypoint correspondences directly affect the pose results. Hence the GPE only mode produces significant jitter. Sometimes it fails to estimate pose when the number of correspondences is insufficient (in our experiments, we only considered 12 or more correspondences after the RANSAC iterations). These shortcomings result in the high residues in both translation and rotation (Fig. 9). The RMS (Root Mean Square) errors of the tracking test for the four objects are presented in Table I. For each object, the upper ones are the results of the GPE only mode and the lower ones are the results of our approach (i.e GPE+LPE). Except the roll angle of the book object, our approach outperforms the GPE only mode in terms of accuracy. Note the significant errors for the cup and the car door objects. The errors are due to limitations of their appearances which stem from the lack of surface texture. This implies that when an object is textureless, the *keypoint-based* method might encounter challenges.

TABLE I: RMS ERRORS.

| | RMS Errors (in meter and degree) | | | | | |
|---|---|---|---|---|---|---|
| | x | y | z | roll | pitch | yaw |
| **Teabox** | 0.0076 | 0.0119 | 0.0355 | 7.90 | 6.01 | 8.73 |
| | **0.0033** | **0.0018** | **0.0068** | **3.27** | **4.32** | **3.95** |
| **Book** | 0.0043 | 0.0030 | 0.0182 | **1.53** | 2.61 | 3.84 |
| | **0.0026** | **0.0021** | **0.0042** | 1.73 | **1.58** | **0.95** |
| **Cup** | 0.0603 | 0.0246 | 0.2687 | 17.50 | 46.58 | 30.35 |
| | **0.0083** | **0.0092** | **0.0272** | **2.09** | **1.83** | **5.05** |
| **Car door** | 0.0502 | 0.0908 | 0.5743 | 51.06 | 17.64 | 23.42 |
| | **0.0211** | **0.0122** | **0.0411** | **1.73** | **3.72** | **3.73** |

### B. Re-initialization Test

During the LPE, it might converge to a local minima because of edge's ambiguity. So monitoring and re-initializing is required to generate a robust tracking system. Here we use a simple heuristic based on the difference in position of the object between frames and the number of valid sample points. When the tracked object drifts, it frequently moves rapidly while the general motions of the object or the camera does not because the frequency in the image acquisition is high[2]. The number of valid sample points also gives a clue to the quality of the pose. Since a good status in LPE implies that most of the sampled points are matched to image edges, we can reason that lots of invalid sample points indicate a risks of tracking failure. In this experiment, we use a criteria when at least one of the xyz coordinates of the object moves more than 10 cm between frames or the number of valid sample points is lower than the half of the total visible sample points, the algorithm switch from the LPE to the GPE and re-

[2]In our implementation, the frame rate is close to 30Hz which means the period is about 33 msec.

initializes. For the test, we intentionally moved the camera to a new scene that does not have the tracked object, shaked the camera rapidly to test on blurred images, and occluded with a paper. Fig. 11 shows the full pose of the book object in the re-initialization test. There are three trials of re-initialization and the invisible spans are shaded in each plot. Since corner features are more easily identified than SURF keypoints in blurred images, the AR marker (i.e. Ground Truth) returns slightly faster than the GPE. This time difference leads to peaks in residue plots (Fig. 12).

### C. Computation Times

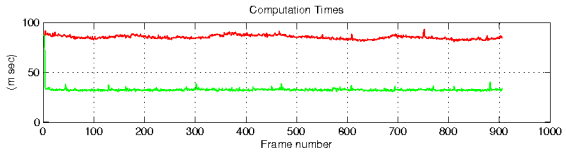


(a) General tracking test

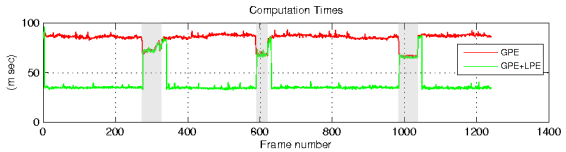


(b) Re-initialization test

Fig. 13: Computation times of the two experimentations of the book object.

For robotic manipulation, higher frame rates are an important requirement. Fig. 13 shows the computation times plot of the two experiments. Since the GPE is executed during re-initializations, our approach (i.e GPE+LPE) takes nearly the same times as the GPE only mode. The reason why the GPE takes less time during re-initialization spans is that the insufficient number of matching skips RANSAC and the pose estimation. The average computation times of the aforementioned experiment is showen in Table II.

TABLE II: AVERAGE COMPUTATION TIMES.

| | GPE (msec) | GPE+LPE (msec) |
|---|---|---|
| **Teabox** | 83.3984 | **32.6695** |
| **Book** | 85.3586 | **32.6478** |
| **Book (re-init)** | 84.5773 | **39.9883** |
| **Cup** | 83.6209 | **43.8241** |
| **Car door** | 94.3990 | **42.4021** |

## VI. Conclusions

We presented a hybrid approach for 3D model-based object tracking. The keypoint-based global pose estimation enabled the proposed system to initialize the tracking system. The edge-based local pose estimation achieves efficient pose tracking. By monitoring the pose results, our system can automatically re-initialize when the tracked results are inconsistent. Since our approach can handle general polygon mesh models, we expect the proposed system can be widely employed for robot manipulation of complex objects.

## VII. Acknowledgments

This work was fully funded and developed under a Collaborative Research Project between Georgia Tech and the General Motors R&D, Manufacturing Systems Research Laboratory on Interaction and Learning for Autonomous Assembly Robots. General Motors support is gratefully acknowledged.

## References

[1] V. Lepetit and P. Fua, "Monocular model-based 3d tracking of rigid objects: A survey," in *Foundations and Trends in Computer Graphics and Vision*, 2005, pp. 1–89.

[2] C. Harris, *Tracking with Rigid Objects*. MIT Press, 1992.

[3] T. Drummond and R. Cipolla, "Real-time visual tracking of complex structures," *IEEE Transactions on Pattern Analysis and Machine Intelligence*, vol. 24, no. 7, pp. 932–946, 2002.

[4] E. Marchand and F. Chaumette, "Virtual visual servoing: a framework for real-time augmented reality," in *Computer Graphics Forum*, vol. 21, 2002, pp. 289–297.

[5] A. I. Comport, E. Marchand, and F. Chaumette, "Robust model-based tracking for robot vision," in *Proceedings of the IEEE/RSJ International Conference on Intelligent Robots and Systems, IROS'04*, vol. 1, 2004.

[6] A. Comport, D. Kragic, E. Marchand, and F. Chaumette, "Robust Real-Time visual tracking: Comparison, theoretical analysis and performance evaluation," in *Proceedings of the IEEE International Conference on Robotics and Automation, ICRA'05*, 2005, pp. 2841–2846.

[7] I. Gordon and D. Lowe, "What and where: 3D object recognition with accurate pose," *Toward Category-Level Object Recognition, (Springer-Verlag)*, pp. 67–82, 2006.

[8] D. G. Lowe, "Distinctive image features from scale-invariant keypoints," *International Journal of Computer Vision*, vol. 60, no. 2, pp. 91–110, 2004.

[9] A. Collet, D. Berenson, S. S. Srinivasa, and D. Ferguson, "Object recognition and full pose registration from a single image for robotic manipulation," in *Proceedings of the IEEE International Conference on Robotics and Automation, ICRA'09*, 2009, pp. 48–55.

[10] M. A. Fischler and R. C. Bolles, "Random sample consensus: a paradigm for model fitting with applications to image analysis and automated cartography," *Commun. ACM*, vol. 24, no. 6, pp. 381–395, 1981.

[11] L. Vacchetti, V. Lepetit, and P. Fua, "Stable real-time 3d tracking using online and offline information," *IEEE Transactions on Pattern Analysis and Machine Intelligence*, vol. 26, no. 10, 2004.

[12] V. Kyrki and D. Kragic, "Integration of model-based and model-free cues for visual object tracking in 3d," in *Proceedings of the IEEE International Conference on Robotics and Automation, ICRA'05*, vol. 2, 2005, pp. 1566–1572.

[13] M. Pressigout and E. Marchand, "Real-time 3d model-based tracking: Combining edge and texture information," in *Proceedings of the IEEE International Conference on Robotics and Automation, ICRA'06*, 2006.

[14] L. Vacchetti, V. Lepetit, and P. Fua, "Combining edge and texture information for real-time accurate 3d camera tracking," in *Third IEEE and ACM International Symposium on Mixed and Augmented Reality, ISMAR'04*, 2004, pp. 48–56.

[15] E. Rosten and T. Drummond, "Fusing points and lines for high performance tracking," in *Tenth IEEE International Conference on Computer Vision, ICCV'05*, vol. 2, 2005.

[16] H. Bay, A. Ess, T. Tuytelaars, and L. V. Gool, "Speeded-up robust features (SURF)," *Computer Vision and Image Understanding*, vol. 110, no. 3, pp. 346–359, 2008.

[17] J. Beis and D. Lowe, "Shape indexing using approximate nearest-neighbour search in high-dimensional spaces," in *IEEE Computer Society Conference on Computer Vision and Pattern Recognition, CVPR'97*, 1997, pp. 1000–1006.

[18] M. Brown and D. G. Lowe, "Unsupervised 3d object recognition and reconstruction in unordered datasets," in *Fifth International Conference on 3-D Digital Imaging and Modeling, 3DIM'05*, 2005, pp. 56–63.

[19] J. Canny, "A computational approach to edge detection," *IEEE Transactions on Pattern Analysis and Machine Intelligence*, pp. 679–698, 1986.